



B-Value Optimization in the Estimation of Intravoxel Incoherent Motion Parameters in Patients with Cervical Cancer

Jose Angelo Udal Perucho, BEng, PhD¹, Hing Chiu Charles Chang, MSc, PhD¹,
Varut Vardhanabhuti, MBBS, BSc, MD Res, FRCR¹, Mandi Wang, MMed¹, Anton Sebastian Becker, MD, PhD²,
Moritz Christoph Wurnig, MD, MSc², Elaine Yuen Phin Lee, MD, BMedSci, BMBS, FRCR¹

¹Department of Diagnostic Radiology, The University of Hong Kong, Hong Kong; ²Institute of Diagnostic and Interventional Radiology, University Hospital of Zurich, Switzerland

Objective: This study aimed to find the optimal number of b-values for intravoxel incoherent motion (IVIM) imaging analysis, using simulated and *in vivo* data from cervical cancer patients.

Materials and Methods: Simulated data were generated using literature pooled means, which served as reference values for simulations. *In vivo* data from 100 treatment-naïve cervical cancer patients with IVIM imaging (13 b-values, scan time, 436 seconds) were retrospectively reviewed. A stepwise b-value fitting algorithm calculated optimal thresholds. Feed forward selection determined the optimal subsampled b-value distribution for biexponential IVIM fitting, and simplified IVIM modeling using monoexponential fitting was attempted. IVIM parameters computed using all b-values served as reference values for *in vivo* data.

Results: In simulations, parameters were accurately estimated with six b-values, or three b-values for simplified IVIM, respectively. *In vivo* data showed that the optimal threshold was 40 s/mm² for patients with squamous cell carcinoma and a subsampled acquisition of six b-values (scan time, 198 seconds) estimated parameters were not significantly different from reference parameters (individual parameter error rates of less than 5%). In patients with adenocarcinoma, the optimal threshold was 100 s/mm², but an optimal subsample could not be identified. Irrespective of the histological subtype, only three b-values were needed for simplified IVIM, but these parameters did not retain their discriminative ability.

Conclusion: Subsampling of six b-values halved the IVIM scan time without significant losses in accuracy and discriminative ability. Simplified IVIM is possible with only three b-values, at the risk of losing diagnostic information.

Keywords: Cervical cancer; Magnetic resonance imaging; Diffusion-weighted imaging; Intravoxel incoherent motion; b-values

INTRODUCTION

Diffusion-weighted imaging (DWI) and apparent diffusion coefficient (ADC) are useful for evaluating and characterizing the primary tumor in cervical cancer (1), assessing metastatic lymph node involvement (2), and monitoring treatment response (3-5). However, the

diffusional signal in cervical cancer is thought to be better ascribed to the intravoxel incoherent motion (IVIM) model (6-9). Previous studies have demonstrated that IVIM could be used to monitor treatment response (10), evaluate hemotoxicity in the bone marrow (11), and predict survival after chemoradiotherapy (10, 12).

It was found that the choice of b-values is the most

Received April 9, 2019; accepted after revision October 30, 2019.

This study was partially supported by the Research Grants Council Hong Kong, General Research Fund (GRF 17119916).

Corresponding author: Elaine Yuen Phin Lee, MD, BMedSci, BMBS, FRCR, Department of Diagnostic Radiology, The University of Hong Kong, Room 406, Block K, Queen Mary Hospital, Pok Fu Lam Road, Hong Kong.

• Tel: (852) 2817-0373 • Fax: (852) 2855-1652 • E-mail: eylee77@hku.hk

This is an Open Access article distributed under the terms of the Creative Commons Attribution Non-Commercial License (<https://creativecommons.org/licenses/by-nc/4.0>) which permits unrestricted non-commercial use, distribution, and reproduction in any medium, provided the original work is properly cited.

crucial parameter affecting ADC calculation (6, 13-16). Furthermore, finding the b-value at which the contribution of perfusion-effects to the diffusional signal is negligible (the so-called fractional b-value) is critical in obtaining a perfusion-insensitive ADC (17, 18). Due to the multi-step estimation process of estimating IVIM parameters, the choice of b-value threshold in the initial estimation of the pure diffusion coefficient (D) and perfusion fraction (f) affects the final fitting (19, 20). Furthermore, the optimal b-value distribution (BVD) and choice of the b-value threshold are organ-specific (19-23).

IVIM protocols typically require more than eight b-values (24, 25). However, these require long acquisition times and are not clinically practical. Hence, for clinical integration, there is a need to reduce the number of b-values acquired. Two strategies have been explored: optimized subsampling and a simplified model. Optimized subsampling takes a subsample of b-values and attempts a biexponential curve fitting; this method has shown good concordance with reference IVIM parameters (26). However, there have been no reports regarding an optimal number of b-values in IVIM in cervical cancer. The simplified model uses a linear fitting, which reduces the number of b-values needed and has demonstrated good concordance with biexponential IVIM. However, the simplified model cannot estimate the pseudo-diffusion coefficient (D*) (27-31).

The purpose of this study was to determine the fractional b-value and explore methods to reduce the number of b-values without sacrificing IVIM estimation accuracy and discriminative ability in cervical cancer.

MATERIALS AND METHODS

Simulations

Simulations were used to evaluate idealized signals for cervical cancer patients and were generated using the IVIM biexponential equation (equation 1a).

$$\frac{S_b}{S_0} = fe^{-b(D + D^*)} + (1 - f)e^{-bD} \quad [1a]$$

Where b is the b-value, S₀ represents the signal obtained at b = 0 s/mm², and S_b represents the signal at a given b-value. IVIM parameters of cervical cancer in the literature (7, 10, 32-34) were used to calculate the pooled parameter means to approach the real case (Table 1).

Two components of Gaussian noise with the same standard deviation (SD) were then added to the signal to simulate a Rician distribution (equation 2).

$$r_b = \sqrt{(s_b + n_{1b})^2 + (n_{2b})^2} \quad [2]$$

Where r_b is the total signal value, s_b is the simulated signal, b is the b-value, and n₁ and n₂ are the two noise components. Two noise levels, SD = 0.1 and 0.01—estimated signal-to-noise ratios (SNR) of 150 and 15 respectively (25)—were analyzed, and 100 signals were generated per noise level (25). The b-values from 0–1000 s/mm² with 25 s/mm² intervals were used. These signals were analyzed with the same pipeline as *in vivo* data.

In Vivo

This retrospective study was approved and performed per the regulations set by the local Institutional Review Board. This study involved anonymized patient data without identifying information that had already been collected, and thus, the need for informed consent was waived.

Data from patients with newly diagnosed cervical cancer (International Federation of Gynecology and Obstetrics [FIGO] stages IB–IVB) with squamous cell carcinoma (SCC) and adenocarcinoma from March 2012 to January 2018 were collected for this study. Exclusion criteria were small tumor size (short axis < 10 mm) and substantial image artifacts shown in the primary tumor. One hundred consecutive patients were included in this study. Portions of the cohort

Table 1. Pooled Analysis of Five Previous Studies for Pooled Means of IVIM Parameters

Studies	n	ADC	D	f	D*
Lee et al., 2014 (7)	16	0.99 ± 0.18	0.86 ± 0.16	0.15 ± 0.03	71.30 ± 10.19
Zhou et al., 2016 (33)	24	0.94 ± 0.06	0.72 ± 0.05	0.20 ± 0.02	23.20 ± 60.00
Zhu et al., 2016 (10)	21	1.00 ± 0.11	0.85 ± 0.12	0.12 ± 0.52	29.23 ± 26.50
Lin et al., 2017 (32)	71	0.87 ± 0.15	0.67 ± 0.11	0.25 ± 0.06	11.51 ± 5.22
Wu et al., 2017 (34)	120	1.10 ± 0.81	0.84 ± 0.27	0.15 ± 0.06	31.50 ± 44.40
Pooled Means	252	0.96 ± 0.03	0.78 ± 0.04	0.19 ± 0.02	33.58 ± 15.38

Values are given as mean ± standard deviation. ADC = apparent diffusion coefficient, D = pure diffusion coefficient, D* = pseudo-diffusion coefficient, f = perfusion fraction, IVIM = intravoxel incoherent motion

have been reported in previous studies (7, 9, 11, 20, 35, 36). Detailed patient demographics can be found in Table 2. *In vivo*, data were analyzed separately according to the histologic subtypes.

Patients selected for the study were those that had fasted at least six hours before the examination, and 20 mg hyoscine butyl bromide (Buscopan, Boehringer Ingelheim, Ingelheim am Rhein, Germany) had been given intravenously to reduce bowel peristalsis. Images were acquired with a 3T MRI system (Achieva 3T TX, Philips Healthcare, Best, the Netherlands) using a dedicated 16-channel phased-array torso coil. DWI utilizing single-shot spin-echo echo-planar imaging was acquired in free-breathing with background body signal suppression. Thirteen b-values (0, 10, 20, 30,

40, 50, 75, 100, 150, 300, 500, 800, and 1000 s/mm²) were acquired, and the total scan time for DWI was 436 seconds. Detailed acquisition parameters can be found in Table 3.

Volumetric regions of interest (VOI) were manually drawn by a board-certified radiologist with 13 years of experience in female pelvic cross-sectional imaging. Areas of hyperintensity on the b1000 maps were taken as the primary tumor, and the radiologist segmented the tumor by referring to a co-registered T2-weighted image and ADC map. These were then copied to a co-registered parametric map. The same task was repeated after a three-month interval for all patients by the same radiologist to test intraobserver reproducibility. The patient order was randomized to reduce recall bias. Another radiologist with two years of experience in pelvic cross-sectional imaging was similarly asked to draw VOIs for all patients to test interobserver reproducibility.

Table 2. Patients' Demographics

Clinical Features	Values
Age (years)	54.61 (21–89)
Tumor size (mm)	48.85 (10.97–101.43)
FIGO staging	
IB	30
IIA	12
IIB	26
IIIA	5
IIIB	25
IVB	2
Histological subtype	
SCC	81
Adenocarcinoma	19
Histological grading	
Well or moderately differentiated	41
Poorly differentiated	59

Values are given as median (range) and counts. FIGO = International Federation of Gynecology and Obstetrics, SCC = squamous cell carcinoma

Table 3. Summary of MRI Scan Parameters

Sequences	T2W TSE	T2W TSE	DWI
Plane	Sagittal	Axial	Axial
TR/TE (ms)	4000/80	2800/100	2000/54
Turbo factor	30	12	NA
SENSE factor	2	2	2
Field of view (mm)	240 x 240	402 x 300	406 x 300
Matrix size	480 x 298	787 x 600	168 x 124
Slice thickness (mm)	4	4	4
Intersection gap (mm)	0	0	0
Bandwidth (Hz/pixel)	230	169	15.3
Number of excitations	2	1	2

DWI = diffusion-weighted imaging, NA = not applicable, SENSE = sensitivity encoding, TR/TE = repetition time/echo time, TSE = turbo spin echo, T2W = T2-weighted

IVIM Analysis Pipeline

Fractional b-Value

An adaptive b-value biexponential fitting algorithm was used to compute the fractional b-value and has been described in detail (19). Briefly, the first step is to calculate D from the highest b-values using a first-order polynomial fit (equation 1b), then calculate f (equation 1c), and finally calculate D*, fixing the computed values of D and f, for all b-values by using a non-linear least squares (NNLS) algorithm and measuring the sum of squared residuals (RSS). These three steps are repeated with the next lower b-value eliminated until only the two highest b-values remain. The b-value threshold with the lowest RSS was considered the fractional b-value.

$$\frac{S_b}{S_0} = e^{-bD} \quad [1b]$$

$$f = \frac{S_b - S_0}{S_b} \quad [1c]$$

Optimal Subsampling

Biexponential IVIM analysis (equation 1a) was performed with the segmented fitting using NNLS. The fractional b-value calculated in the previous section was used as the optimal b-value threshold. The first three b-values were determined by testing all combinations of three b-values, and the combination with the lowest total parameter error (TPE) was then fixed for subsequent iterations. TPE is

defined by equation 3a.

$$TPE = \frac{\sqrt{\frac{1}{N} \sum_s^2 (D_s - D_p)^2}}{D_p} + \frac{\sqrt{\frac{1}{N} \sum_s^2 (f_s - f_p)^2}}{f_p} + \frac{\sqrt{\frac{1}{N} \sum_s^2 (D_s^* - D_p^*)^2}}{D_p^*} \quad [3a]$$

Where N represents the number of signals, D_s , f_s , and D_s^* represent the subsampled IVIM estimates and D_p , f_p , and D_p^* represent the pooled parameter means. Then, for each incremental distribution size, the optimal b-values were determined by feed forward selection. Unfixed b-values were sampled, and the b-value whose inclusion led to the lowest TPE was fixed for subsequent iterations; this was repeated until all b-values were added. TPE for *in vivo* data is defined by equation 3b.

$$TPE = \frac{1}{N} \sum_i^1 \sqrt{\left(\frac{D_i - D_r}{D_r}\right)^2} + \frac{1}{N} \sum_i^1 \sqrt{\left(\frac{f_i - f_r}{f_r}\right)^2} + \frac{1}{N} \sum_i^1 \sqrt{\left(\frac{D_i^* - D_r^*}{D_r^*}\right)^2} \quad [3b]$$

Where N represents the number of patients, D_i , f_i , and D_i^* represent the subsampled IVIM estimates, and D_r , f_r , and D_r^* represent the reference IVIM estimates from the full 13 BVD. Fit quality per unit time (FQPUT) for *in vivo* data was also measured and was defined as the decrease of parameter error divided by the increase in scan time.

Simplified IVIM

Under the assumption that $D^* > D$ (37), equation 1a can be simplified to equation 4 at high b-values (30):

$$\frac{S_b}{S_0} = (1 - f)e^{-bD} \quad [4]$$

The optimal simplified IVIM BVD was also determined in a feed forward fashion.

Statistical Analysis

All simulations, IVIM, and statistical analysis were done using MATLAB (The Mathworks Inc., Natick, MA, USA). The two-sample Mann-Whitney U test was used to compare the optimal b-value thresholds between the SCC and adenocarcinoma and to compare the IVIM parameters between histological grading and FIGO staging. FIGO stages were dichotomized into low (IB–IIA) and high (IIA–IVB) stages.

For simulated data, the estimated biexponential parameters (denoted as $D_{\text{subsampled}}$, $f_{\text{subsampled}}$, and $D^*_{\text{subsampled}}$) and simplified parameters (denoted as D_{linear} and f_{linear}) were compared with the pooled means IVIM parameters (denoted as $D_{\text{reference}}$, $f_{\text{reference}}$, $D^*_{\text{reference}}$) using the one-sample Mann-Whitney U test at all subsample sizes. For *in vivo* data, the

estimated biexponential and simplified parameters were compared with the reference IVIM parameters calculated by the full 13 BVD (denoted as $D_{\text{reference}}$, $f_{\text{reference}}$, $D^*_{\text{reference}}$) using the two-sample Mann-Whitney U test at all subsample sizes.

Intraclass correlation coefficient (ICC) was used to assess interobserver and intraobserver reproducibility of parameters derived from the reference, subsampled, and simplified models. Values of 0.50–0.75, 0.76–0.90, and > 0.90 are considered to indicate moderate, good, and excellent consistency, respectively.

RESULTS

Optimal b-Value Threshold

For simulated data, the optimal b-value threshold was 25 s/mm^2 . For SCC, the median threshold was 40 s/mm^2 , and it was 100 s/mm^2 for adenocarcinoma (Fig. 1). Thus, 100 s/mm^2 was taken as the optimal *in vivo* threshold.

Optimal Subsampling

The optimal three BVD was (0, 200, 1000) s/mm^2 for simulated data and (0, 300, 1000) s/mm^2 for *in vivo* data, regardless of the histological subtype (Supplementary Fig. 1).

In both simulated and *in vivo* data, the TPE of biexponential IVIM (TPE_{bIVIM}) decreased as more b-values were added (Fig. 2). Perfusion-related parameter errors

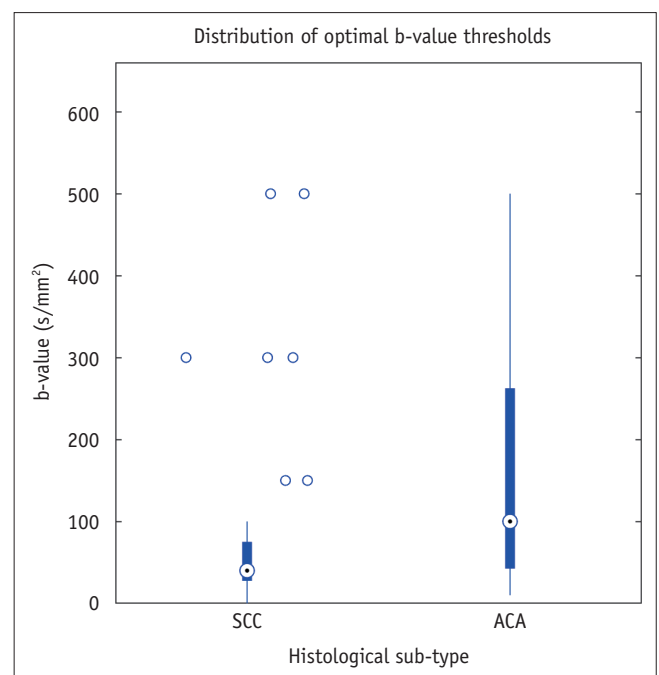


Fig. 1. Distribution of optimal b-value thresholds for *in vivo* data. ACA = adenocarcinoma, SCC = squamous cell carcinoma

were acceptable in low-noise simulated and *in vivo* data but were high in high-noise simulated data, with errors over 500%. Hence, high-noise simulations were deemed not representative of the clinical routine and excluded from further analysis.

In low-noise simulations, subsampled parameters were not significantly different from the respective pooled means parameters at all distribution sizes greater than four (Supplementary Table 1). The optimal protocol included six b-values, (0, 25, 100, 175, 200, 1000) s/mm², which had D, f, and D* errors of 3.63%, 0.36%, and 0.09%, respectively and were not significantly different from the reference parameters ($p = 0.141$, $p = 0.907$, $p = 0.474$).

In vivo, subsampled parameters in SCC were not significantly different from reference parameters from a distribution size of six. FQPUT also plateaued at six b-values (Supplementary Fig. 2). The optimal subsampled protocol

included six b-values, (0, 10, 30, 75, 300, 1000) s/mm² and had D, f, and D* errors of 0.33%, 4.11%, and 3.49%, respectively, that were not significantly different from the reference parameters ($p = 1.000$, $p = 0.378$, $p = 0.981$). This scan time decreased to 198 seconds, representing a 55% scan time reduction. For adenocarcinoma, D_{subsampled} was not significantly different from D_{reference} at all distribution sizes greater than 4 (Supplementary Table 1), but the trends for f_{subsampled} and D*_{subsampled} were not consistent, leaving no optimal subsampled BVD.

Simplified IVIM

For low noise simulations, the optimal three BVD was (0, 200, 1000) s/mm², which achieved D and f errors of 167.25% and 546.61%, respectively (Supplementary Fig. 3). However, the TPE of the simplified IVIM model (TPE_{IVIM}) was high, and consequently, the simplified parameters were

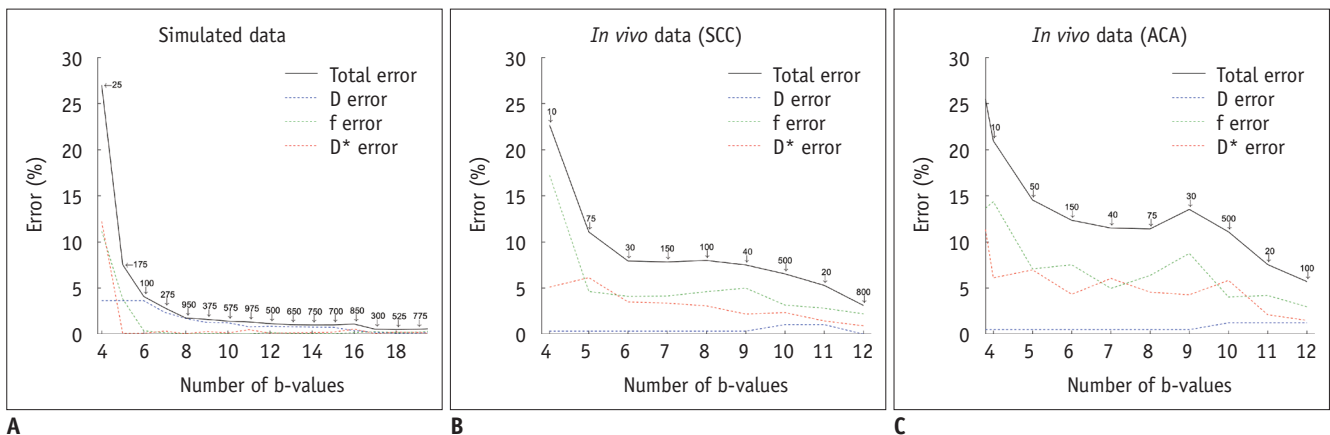


Fig. 2. Evolution of total IVIM parameter error as more b-values were added in (A) low noise simulated signals (truncated to 20 b-values) as well as *in vivo* data for patients with (B) SCC and (C) ACA. Annotated numbers on total error curves represent which b-value was added at that iteration of feed forward selection loop. D = pure diffusion coefficient, D* = pseudo-diffusion coefficient, f = perfusion fraction, IVIM = intravoxel incoherent motion

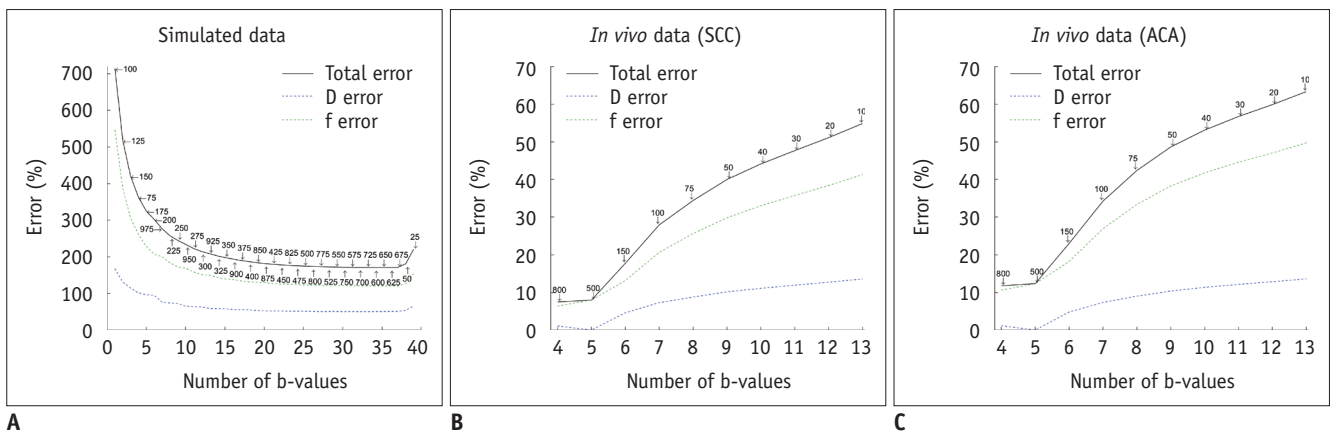


Fig. 3. Evolution of total simplified IVIM parameter error as more b-values were sampled in (A) low noise simulated signals as well as *in vivo* data for patients with (B) SCC, and (C) ACA. Annotated numbers on total error curves represent which b-value was added at that iteration of feed forward selection loop.

significantly different from the pooled mean parameters ($p < 0.001$) at all distribution sizes (Supplementary Table 2).

For *in vivo* data, the TPE_{sIVIM} was low when only high b-values, i.e., b-values greater than the fractional b-value, were sampled (Fig. 3). In SCC, the optimal choice for a three BVD was (0, 300, 1000) s/mm², which achieved D and f errors of 1.10% and 6.30%, respectively, and was not significantly different from the reference parameters ($p = 0.229$, $p = 0.089$). Adenocarcinoma also had the same optimal choice of BVD and had D and f errors of 1.18% and 10.59%, respectively, and was also not significantly different from the reference parameters ($p = 0.623$, $p = 0.212$). The scan time decreased to 99 seconds, representing a 77% scan time reduction.

Interobserver and Intraobserver Reproducibility

Interobserver reproducibility of IVIM parameters was good, while intraobserver reproducibility was excellent (Table 4). Values of f were slightly less reproducible compared to values of D while D* had the highest reproducibility.

Associations with Clinicopathologic Factors

In SCC, $f_{reference}$ and $f_{subsampled}$ were found to be significantly different between histological grades, and $D^*_{reference}$ and $D^*_{subsampled}$ were found to be significantly different between FIGO groups (Table 5). In adenocarcinoma, f_{linear} was significantly different between histological grades. In both SCC and adenocarcinoma, neither the subsampled nor

simplified IVIM parameters were significantly different from the reference parameters regardless of histological and staging groups (Table 6).

DISCUSSION

In the current study, we examined whether the number of b-values can be reduced without sacrificing the precision of the IVIM parameter estimates in DWI of cervical cancer. We found that a subsampled distribution of six b-values yielded IVIM parameters with an error of around 4% while preserving the discriminative ability between histological grades and FIGO groups in patients with SCC. Even though three b-values were enough for a simplified model and D_{linear} and f_{linear} had an error rate of 1% and 8%, respectively, in our study, this model could not retain its discriminative property.

In the estimation of IVIM parameters, segmented fitting is used to reduce error (38). This multi-step process requires a b-value threshold to be selected, and several studies have demonstrated the importance of choosing an appropriate threshold (22, 39). However, it was also found that the threshold is dependent on the organs, with values ranging from 20 s/mm² in the healthy liver (19) to 300 s/mm² in breast cancer (23). In the present study, we found that the optimal threshold for SCC was 40 s/mm² and 100 s/mm² for adenocarcinoma, which was similar to a previous report (20).

For the determination of an optimal BVD for cervical cancer using simulations, acceptable TPE_{bIVIM} was achieved after 4 b-values were sampled and reached a minimum with 18 b-values. Two other optimization simulation studies suggested a distribution size of 8 to 16 b-values (24, 25). In high noise simulated signals, SNR of 15, perfusion parameters could not be accurately estimated, in contrast with a study that suggested a minimum SNR of 8 (24). The feed forward algorithm used in this study determined a clustered distribution to produce the lowest errors in concordance with a study in which clustered distributions had better measurement consistency compared with equally-spaced distributions (25).

Considering that one limiting factor for the clinical translation of IVIM is the long scan time, reducing the number of b-values needed could promote the clinical integration of IVIM. It was found that the TPE_{bIVIM} steadily decreased in SCC, and parameter errors were below 5% using six b-values. Furthermore, both $f_{reference}$ and $f_{subsampled}$ were significantly different between histological grading

Table 4. Interobserver and Intraobserver Variability

Parameters	Interobserver ICC	Intraobserver ICC
Reference		
D	0.79	0.89
f	0.78	0.81
D*	0.95	0.94
Subsampled		
D	0.77	0.91
f	0.70	0.86
D*	0.95	0.95
Simplified		
D	0.79	0.89
f	0.74	0.80

Interobserver and intraobserver variability was measured with ICC of IVIM parameters derived from biexponential model using all 13 b-values (reference), biexponential model using optimized subsample of 6 b-values (subsampled), and monoexponential model using optimized distribution of 3 b-values (simplified). ICC = intraclass correlation coefficient

and that both $D^*_{reference}$ and $D^*_{subsampled}$ were significantly different between FIGO stages in SCC, implying that the subsampled parameters had similar discriminative abilities as the reference parameters. While it was observed that the TPE_{bIVIM} decreased in adenocarcinomas, the trends for the perfusion parameters were erratic, and errors remained high up to 10 b-values, suggesting that IVIM imaging may not be a proper modality to assess cervical adenocarcinoma.

In selecting the minimum number of b-values, FQPUT balances accuracy with acquisition time (24, 40). In SCC, FQPUT plateaued at six b-values, which potentially represents a minimum acquisition for biexponential analysis, reducing the scan time by as much as 55%. In comparison, liver studies have found that the FQPUT plateaus at around eight b-values (24, 26). However, it has been suggested that the liver was better described by a multiexponential

Table 5. IVIM Parameters

Parameters	All Patients	Histological Grading			FIGO Staging		
		WD/MD	PD	P	Low (IB–IIA)	High (IIA–IVB)	P
SCC							
$D_{reference}^\dagger$	0.845 ± 0.178	0.842 ± 0.165	0.847 ± 0.118	0.621	0.836 ± 0.167	0.850 ± 0.116	0.329
$f_{reference}$	0.142 ± 0.027	0.133 ± 0.017	0.147 ± 0.031	0.023*	0.145 ± 0.035	0.139 ± 0.021	0.714
$D^*_{reference}^\dagger$	53.74 ± 5.652	55.01 ± 4.562	52.91 ± 6.165	0.185	51.97 ± 6.081	54.90 ± 5.089	0.026*
$D_{subsampled}^\dagger$	0.845 ± 0.138	0.843 ± 0.166	0.847 ± 0.118	0.676	0.836 ± 0.168	0.851 ± 0.116	0.301
$f_{subsampled}$	0.139 ± 0.030	0.130 ± 0.018	0.145 ± 0.035	0.042*	0.143 ± 0.039	0.137 ± 0.022	0.770
$D^*_{subsampled}^\dagger$	53.74 ± 6.004	55.14 ± 4.818	52.83 ± 6.553	0.195	51.71 ± 6.777	55.07 ± 5.083	0.017*
D_{linear}^\dagger	0.845 ± 0.138	0.843 ± 0.166	0.847 ± 0.118	0.676	0.836 ± 0.168	0.851 ± 0.116	0.301
f_{linear}	0.140 ± 0.032	0.132 ± 0.020	0.145 ± 0.038	0.112	0.143 ± 0.042	0.138 ± 0.024	0.920
Adenocarcinoma							
$D_{reference}^\dagger$	0.893 ± 0.140	0.944 ± 0.124	0.848 ± 0.144	0.156	0.859 ± 0.119	0.931 ± 0.159	0.211
$f_{reference}$	0.145 ± 0.028	0.156 ± 0.022	0.135 ± 0.031	0.113	0.143 ± 0.037	0.147 ± 0.016	0.905
$D^*_{reference}^\dagger$	49.46 ± 6.075	50.66 ± 7.331	48.39 ± 4.831	0.211	51.77 ± 6.150	46.90 ± 5.140	0.133
D_{linear}^\dagger	0.892 ± 0.140	0.944 ± 0.126	0.847 ± 0.142	0.133	0.859 ± 0.119	0.931 ± 0.158	0.182
f_{linear}	0.140 ± 0.034	0.157 ± 0.033	0.125 ± 0.029	0.043*	0.146 ± 0.044	0.134 ± 0.019	0.720

Values are given as mean ± standard deviation. IVIM parameters were derived from biexponential fitting of all available 13 b-values (reference), biexponential fitting of optimal subsampled b-value distribution (subsampled), and monoexponential fitting of optimal sIVIM model (linear), separated by histological grading, and FIGO staging. * $p < 0.05$, † Values in units of $\times 10^{-3} \text{ mm}^2/\text{s}$. MD = moderately differentiated, PD = poorly differentiated, sIVIM = simplified IVIM, WD = well differentiated

Table 6. Comparisons of IVIM Parameters

Parameters	Histological Grading				FIGO Staging			
	WD/MD	P	PD	P	Low (IB–IIA)	P	High (IIA–IVB)	P
SCC								
$D_{reference}^\dagger$	0.842 ± 0.165	ref	0.847 ± 0.118	ref	0.836 ± 0.167	ref	0.850 ± 0.116	ref
$D_{subsampled}^\dagger$	0.843 ± 0.166	0.899	0.847 ± 0.118	0.983	0.836 ± 0.168	0.963	0.851 ± 0.116	0.949
D_{linear}^\dagger	0.843 ± 0.166	0.899	0.847 ± 0.118	0.983	0.836 ± 0.168	0.963	0.851 ± 0.116	0.949
$f_{reference}$	0.133 ± 0.017	ref	0.147 ± 0.031	ref	0.145 ± 0.035	ref	0.139 ± 0.021	ref
$f_{subsampled}$	0.130 ± 0.018	0.580	0.145 ± 0.035	0.502	0.143 ± 0.039	0.589	0.137 ± 0.022	0.471
f_{linear}	0.132 ± 0.020	0.899	0.145 ± 0.038	0.552	0.143 ± 0.042	0.553	0.138 ± 0.024	0.778
$D^*_{reference}^\dagger$	55.01 ± 4.562	ref	52.91 ± 6.165	ref	51.97 ± 6.081	ref	54.90 ± 5.089	ref
$D^*_{subsampled}^\dagger$	55.14 ± 4.818	0.989	52.83 ± 6.553	0.989	51.71 ± 6.777	1.000	55.07 ± 5.083	0.966
Adenocarcinoma								
$D_{reference}^\dagger$	0.944 ± 0.124	ref	0.848 ± 0.144	ref	0.859 ± 0.119	ref	0.931 ± 0.159	ref
D_{linear}^\dagger	0.944 ± 0.126	0.899	0.847 ± 0.142	0.983	0.859 ± 0.119	0.963	0.931 ± 0.158	0.949
$f_{reference}$	0.156 ± 0.022	ref	0.135 ± 0.031	ref	0.143 ± 0.037	ref	0.147 ± 0.016	ref
f_{linear}	0.157 ± 0.033	0.899	0.125 ± 0.029	0.552	0.146 ± 0.044	0.553	0.134 ± 0.019	0.788

Statistical comparisons were performed for IVIM parameters IVIM parameters were estimated from biexponential fitting of optimal subsampled b-value distribution (subsampled) and monoexponential fitting of optimal sIVIM model (linear) against biexponential fitting of all available 13 b-values (reference), separated by histological grading, and FIGO staging. † Values in units of $\times 10^{-3} \text{ mm}^2/\text{s}$.

model (41) due to the dual flow nature of the liver (42), so more b-values may be required.

Another approach for reducing the acquisition and post-processing time of IVIM is the use of a simplified model (30). Linear fitting requires fewer sampled b-values and lower post-processing intensity. Even though this simplified method precludes the calculation of D^* , it is unclear whether D^* can serve as a clinically relevant parameter due to its high variability (31).

The simulation experiments demonstrated that TPE_{sIVIM} was high regardless of distribution size. In contrast, *in vivo* experiments could estimate parameters that were not significantly different from those calculated by the biexponential model. In the case of simulated signals, Gaussian noise was added, so sampling more b-values was a compensatory step to reduce the disparity between the estimated and the pooled means parameters. However, in the case of *in vivo* data, the reference values were from the 13 b-values using a biexponential fit, so sampling more b-values was not needed. Previous studies have also shown that the simplified method yields estimates close to biexponential fitting with only three b-values in brain pathologies (28) and pancreatic (31) and head and neck cancers (27).

In choosing the b-values for simplified IVIM, the choice of b_{Low} affected TPE_{sIVIM} more than the choice of b_{High} . It was also observed that sampling low b-values increased parameter error as it pushed the slope to be artificially steeper due to perfusion effects. It was previously suggested that all non-zero b-values be greater than the fractional b-value (17). Sampling more high b-values appeared to slightly increase TPE_{sIVIM} in contrast with a previous study (28). Despite the low errors achieved using this model, f_{linear} could not be used to separate histological grades in SCC. Though f_{linear} was shown to be significantly different between grades in adenocarcinoma, this is a false positive as $f_{reference}$ was not significantly different, suggesting that the simplified model may not be clinically relevant in cervical cancer.

ICC testing of reference, subsampled, and simplified IVIM parameters demonstrated good interobserver and intraobserver reproducibility. Interestingly, D^* was shown to have high reproducibility, which may be because many voxels had calculated values that were beyond the constraints set.

This study has several limitations. First, interscanner and interprotocol variations have not been tested. Therefore,

a multi-center study may be necessary to generalize these results. Second, as this was a retrospective study, the choice of b-values for patients was not guided by simulation results. Lastly, the feed forward approach used in this study saves computation time by reducing the search space compared to an exhaustive grid search but may not find the true minimum at a given subsample size.

In summary, by using the optimized BVD, the proposed method could reduce IVIM scan time by 55% with a low error rate, estimating parameters that were not significantly different from reference parameters. Furthermore, both $f_{reference}$ and $f_{subsampled}$ were significantly different between histological grades, while both $D^*_{reference}$ and $D^*_{subsampled}$ were significantly different between FIGO stages in patients with SCC. Therefore, optimized subsampling may potentially allow the integration of IVIM in a clinical setting for patients with cervical cancer.

Supplementary Materials

The Data Supplement is available with this article at <https://doi.org/10.3348/kjr.2019.0232>.

Conflicts of Interest

The authors have no potential conflicts of interest to disclose.

ORCID iDs

Elaine Yuen Phin Lee

<https://orcid.org/0000-0002-0627-5297>

Jose Angelo Udal Perucho

<https://orcid.org/0000-0001-6088-3173>

Hing Chiu Charles Chang

<https://orcid.org/0000-0001-8634-328X>

Varut Vardhanabhuti

<https://orcid.org/0000-0001-6677-3194>

Mandi Wang

<https://orcid.org/0000-0002-8467-148X>

Anton Sebastian Becker

<https://orcid.org/0000-0001-8372-6496>

Moritz Christoph Wurnig

<https://orcid.org/0000-0001-7865-4010>

REFERENCES

1. McVeigh PZ, Syed AM, Milosevic M, Fyles A, Haider MA. Diffusion-weighted MRI in cervical cancer. *Eur Radiol*

- 2008;18:1058-1064
2. Xue HD, Li S, Sun F, Sun HY, Jin ZY, Yang JX, et al. Clinical application of body diffusion weighted MR imaging in the diagnosis and preoperative N staging of cervical cancer. *Chin Med Sci J* 2008;23:133-137
 3. Patterson DM, Padhani AR, Collins DJ. Technology insight: water diffusion MRI—a potential new biomarker of response to cancer therapy. *Nat Clin Pract Oncol* 2008;5:220-233
 4. Koh DM, Takahara T, Imai Y, Collins DJ. Practical aspects of assessing tumors using clinical diffusion-weighted imaging in the body. *Magn Reson Med Sci* 2007;6:211-224
 5. Harry VN, Semple SI, Gilbert FJ, Parkin DE. Diffusion-weighted magnetic resonance imaging in the early detection of response to chemoradiation in cervical cancer. *Gynecol Oncol* 2008;111:213-220
 6. Kallehauge JF, Tanderup K, Haack S, Nielsen T, Muren LP, Fokdal L, et al. Apparent diffusion coefficient (ADC) as a quantitative parameter in diffusion weighted MR imaging in gynecologic cancer: dependence on b-values used. *Acta Oncol* 2010;49:1017-1022
 7. Lee EY, Yu X, Chu MM, Ngan HY, Siu SW, Soong IS, et al. Perfusion and diffusion characteristics of cervical cancer based on intravoxel incoherent motion MR imaging—a pilot study. *Eur Radiol* 2014;24:1506-1513
 8. Le Bihan D, Breton E, Lallemand D, Aubin ML, Vignaud J, Laval-Jeantet M. Separation of diffusion and perfusion in intravoxel incoherent motion MR imaging. *Radiology* 1988;168:497-505
 9. Lee EY, Hui ES, Chan KK, Tse KY, Kwong WK, Chang TY, et al. Relationship between intravoxel incoherent motion diffusion-weighted MRI and dynamic contrast-enhanced MRI in tissue perfusion of cervical cancers. *J Magn Reson Imaging* 2015;42:454-459
 10. Zhu L, Zhu L, Shi H, Wang H, Yan J, Liu B, et al. Evaluating early response of cervical cancer under concurrent chemo-radiotherapy by intravoxel incoherent motion MR imaging. *BMC Cancer* 2016;16:79
 11. Lee EYP, Perucho JAU, Vardhanabhuti V, He J, Siu SWK, Ngu SF, et al. Intravoxel incoherent motion MRI assessment of chemoradiation-induced pelvic bone marrow changes in cervical cancer and correlation with hematological toxicity. *J Magn Reson Imaging* 2017;46:1491-1498
 12. Zhu L, Wang H, Zhu L, Meng J, Xu Y, Liu B, et al. Predictive and prognostic value of intravoxel incoherent motion (IVIM) MR imaging in patients with advanced cervical cancers undergoing concurrent chemo-radiotherapy. *Sci Rep* 2017;7:11635
 13. Ogura A, Tamura T, Ozaki M, Doi T, Fujimoto K, Miyati T, et al. Apparent diffusion coefficient value is not dependent on magnetic resonance systems and field strength under fixed imaging parameters in brain. *J Comput Assist Tomogr* 2015;39:760-765
 14. Dale BM, Braithwaite AC, Boll DT, Merkle EM. Field strength and diffusion encoding technique affect the apparent diffusion coefficient measurements in diffusion-weighted imaging of the abdomen. *Invest Radiol* 2010;45:104-108
 15. Habermann CR, Gossrau P, Kooijman H, Graessner J, Cramer MC, Kaul MG, et al. Monitoring of gustatory stimulation of salivary glands by diffusion-weighted MR imaging: comparison of 1.5T and 3T. *AJNR Am J Neuroradiol* 2007;28:1547-1551
 16. Matsuoka A, Minato M, Harada M, Kubo H, Bandou Y, Tangoku A, et al. Comparison of 3.0- and 1.5-tesla diffusion-weighted imaging in the visibility of breast cancer. *Radiat Med* 2008;26:15-20
 17. Ogura A, Hatano I, Osakabe K, Yamaguchi N, Koyama D, Watanabe H. Importance of fractional b value for calculating apparent diffusion coefficient in DWI. *AJR Am J Roentgenol* 2016;207:1239-1243
 18. Freiman M, Voss SD, Mulkern RV, Perez-Rossello JM, Callahan MJ, Warfield SK. *In vivo* assessment of optimal b-value range for perfusion-insensitive apparent diffusion coefficient imaging. *Med Phys* 2012;39:4832-4839
 19. Wurnig MC, Donati OF, Ulbrich E, Filli L, Kenkel D, Thoeny HC, et al. Systematic analysis of the intravoxel incoherent motion threshold separating perfusion and diffusion effects: proposal of a standardized algorithm. *Magn Reson Med* 2015;74:1414-1422
 20. Becker AS, Perucho JA, Wurnig MC, Boss A, Ghafoor S, Khong PL, et al. Assessment of cervical cancer with a parameter-free intravoxel incoherent motion imaging algorithm. *Korean J Radiol* 2017;18:510-518
 21. Pang Y, Turkbey B, Bernardo M, Kruecker J, Kadoury S, Merino MJ, et al. Intravoxel incoherent motion MR imaging for prostate cancer: an evaluation of perfusion fraction and diffusion coefficient derived from different b-value combinations. *Magn Reson Med* 2013;69:553-562
 22. Koh DM, Collins DJ, Orton MR. Intravoxel incoherent motion in body diffusion-weighted MRI: reality and challenges. *AJR Am J Roentgenol* 2011;196:1351-1361
 23. Chen W, Zhang J, Long D, Wang Z, Zhu JM. Optimization of intra-voxel incoherent motion measurement in diffusion-weighted imaging of breast cancer. *J Appl Clin Med Phys* 2017;18:191-199
 24. Lemke A, Stieltjes B, Schad LR, Laun FB. Toward an optimal distribution of b values for intravoxel incoherent motion imaging. *Magn Reson Imaging* 2011;29:766-776
 25. Jambor I, Merisaari H, Aronen HJ, Järvinen J, Saunavaara J, Kauko T, et al. Optimization of b-value distribution for biexponential diffusion-weighted MR imaging of normal prostate. *J Magn Reson Imaging* 2014;39:1213-1222
 26. Dyvorne H, Jajamovich G, Kakite S, Kuehn B, Taouli B. Intravoxel incoherent motion diffusion imaging of the liver: optimal b-value subsampling and impact on parameter precision and reproducibility. *Eur J Radiol* 2014;83:2109-2113
 27. Sasaki M, Sumi M, Eida S, Katayama I, Hotokezaka Y, Nakamura T. Simple and reliable determination of intravoxel incoherent motion parameters for the differential diagnosis of head and neck tumors. *PLoS One* 2014;9:e112866

28. Conklin J, Heyn C, Roux M, Cerny M, Wintermark M, Federau C. A simplified model for intravoxel incoherent motion perfusion imaging of the brain. *AJNR Am J Neuroradiol* 2016;37:2251-2257
29. Pieper CC, Sprinkart AM, Meyer C, König R, Schild HH, Kukuk GM, et al. Evaluation of a simplified intravoxel incoherent motion (IVIM) analysis of diffusion-weighted imaging for prediction of tumor size changes and imaging response in breast cancer liver metastases undergoing radioembolization: a retrospective single center analysis. *Medicine (Baltimore)* 2016;95:e3275
30. Pekar J, Moonen CTW, van Zijl PCM. On the precision of diffusion/perfusion imaging by gradient sensitization. *Magn Reson Med* 1992;23:122-129
31. Concia M, Sprinkart AM, Penner AH, Brossart P, Gieseke J, Schild HH, et al. Diffusion-weighted magnetic resonance imaging of the pancreas: diagnostic benefit from an intravoxel incoherent motion model-based 3 b-value analysis. *Invest Radiol* 2014;49:93-100
32. Lin M, Yu X, Chen Y, Ouyang H, Wu B, Zheng D, et al. Contribution of mono-exponential, bi-exponential and stretched exponential model-based diffusion-weighted MR imaging in the diagnosis and differentiation of uterine cervical carcinoma. *Eur Radiol* 2017;27:2400-2410
33. Zhou Y, Liu J, Liu C, Jia J, Li N, Xie L, et al. Intravoxel incoherent motion diffusion weighted MRI of cervical cancer—Correlated with tumor differentiation and perfusion. *Magn Reson Imaging* 2016;34:1050-1056
34. Wu Q, Wang Y, Shi L, Dong L, Liu M, Dou S, et al. Intravoxel incoherent motion diffusion-weighted magnetic resonance imaging of cervical cancer with different b-values. *J Comput Assist Tomogr* 2017;41:592-598
35. Becker AS, Ghafoor S, Marcon M, Perucho JA, Wurnig MC, Wagner MW, et al. MRI texture features may predict differentiation and nodal stage of cervical cancer: a pilot study. *Acta Radiol Open* 2017;6:2058460117729574
36. Lai AYT, Perucho JAU, Xu X, Hui ES, Lee EYP. Concordance of FDG PET/CT metabolic tumour volume versus DW-MRI functional tumour volume with T2-weighted anatomical tumour volume in cervical cancer. *BMC Cancer* 2017;17:825
37. Le Bihan D, Turner R, MacFall JR. Effects of intravoxel incoherent motions (IVIM) in steady-state free precession (SSFP) imaging: application to molecular diffusion imaging. *Magn Reson Med* 1989;10:324-337
38. Sigmund EE, Cho GY, Kim S, Finn M, Moccaldi M, Jensen JH, et al. Intravoxel incoherent motion imaging of tumor microenvironment in locally advanced breast cancer. *Magn Reson Med* 2011;65:1437-1447
39. Chandarana H, Lee VS, Hecht E, Taouli B, Sigmund EE. Comparison of biexponential and monoexponential model of diffusion weighted imaging in evaluation of renal lesions: preliminary experience. *Invest Radiol* 2011;46:285-291
40. Tan PN, Steinbach M, Kumar V. *Introduction to data mining*, 1st ed. Boston, MA: Pearson Addison Wesley, 2005
41. Wurnig MC, Germann M, Boss A. Is there evidence for more than two diffusion components in abdominal organs?—A magnetic resonance imaging study in healthy volunteers. *NMR Biomed* 2018;31:e3852
42. Molmenti EP, Levy MF, Molmenti H, Casey D, Fasola CG, Hamilton WM, et al. Correlation between intraoperative blood flows and hepatic artery strictures in liver transplantation. *Liver Transpl* 2002;8:160-163